

Appendix A: [OI] $\lambda 6300$ LVC line profiles and luminosities for the X-shooter sample

Appendix A.1: Line profiles and luminosities

Table A.1 lists the [OI] $\lambda 6300$ LVC fit parameters for the X-shooter sample. Figure A.1 shows the fitted [OI] $\lambda 6300$ line profiles for the X-shooter sample. Figure A.2 shows the kinematic properties of the [OI] $\lambda 6300$ line for the X-shooter sample. Figure A.3 shows the kinematic properties as a function of projected separation from σ -Ori.

Appendix A.2: Comparison with MIKE observations

Figure A.4 shows the comparison between the X-shooter and the MIKE spectra for the overlapping sample.

Appendix B: $L_{\text{[OI]}} - L_{\text{acc}}$ fit: corner plots and bootstrapping method

We show in Figures B.1 and B.2 the corner plots showing the intercept, slope, standard deviation, and correlation coefficient for the fit of the $\log L_{\text{OI,LVC}}$ vs. $\log L_{\text{acc}}$ relation (see sect. 6.2.1, Fig. 5). This is done using `linmix` (Kelly 2007), considering data with detection on both axes, and including upper limits.

We show the bootstrapping method applied to the $\log L_{\text{OI,LVC}}$ vs. $\log L_{\text{acc}}$ relationship in Fig. B.3. Following Aru et al. (2024); McLeod et al. (2021), we use a bootstrap sampling method with 10^4 iterations, where we randomize the x-values ($\log L_{\text{acc}}$) and compute the Spearman correlation coefficient. Secondly, we assess the uncertainty of the correlation coefficient by bootstrapping with 10^4 iterations while varying the y-axis values ($\log L_{\text{OI,LVC}}$) within their respective uncertainties taken as the standard deviation of a Gaussian distribution of random points, for both the far and near samples. These tests are then compared with the actual Spearman correlation coefficient r_s . The left panel of Fig. B.3 shows the test for the far sample while the right panel shows it for the near sample. We show that the Spearman correlation coefficient for the measured data (orange line), lies outside 2σ of the randomized distribution for the far sample, i.e., $\log L_{\text{OI,LVC}}$ and $\log L_{\text{acc}}$ are correlated, while the observed Spearman correlation coefficient as well as both histograms are similar for the near sample, i.e., $\log L_{\text{OI,LVC}}$ and $\log L_{\text{acc}}$ are not correlated.

Appendix C: The [NII] $\lambda 6583$ and [SII] $\lambda 6731$, [SII] $\lambda 6716$ forbidden lines

Appendix C.1: Line profiles fits

This section presents the fit results for the [NII] $\lambda 6583$, [SII] $\lambda 6716$, and [SII] $\lambda 6731$ forbidden lines for the MIKE and X-shooter samples. For the MIKE sample, Tables C.1, C.2, and C.3 list the fit results for the [NII] $\lambda 6583$, [SII] $\lambda 6731$, and [SII] $\lambda 6716$ lines, respectively. The line profiles, with their corresponding Gaussian components fits, are shown in Figures C.1, C.2, and C.3.

For the X-shooter sample, Tables C.4, C.5, and C.6 list the fit results for the [NII] $\lambda 6583$, [SII] $\lambda 6731$, and [SII] $\lambda 6716$ lines, respectively. The line profiles, with their corresponding Gaussian components fits, are shown in Figures C.4, C.5, and Figures C.6.

Appendix C.2: Line kinematics with respect to projected distance to σ -Ori

The kinematic properties of the lines (v_{peak} , FWHM) as a function of the projected separation to the massive system σ -Ori are shown in Figures C.7 and C.8 for [NII] $\lambda 6583$ and [SII] $\lambda 6731$ lines respectively, as observed in our MIKE sample, and in Figures C.9 and C.10 for [NII] $\lambda 6583$ and [SII] $\lambda 6731$ lines respectively, in the X-shooter sample.

Appendix D: High-velocity components fits

This section presents the fit results for the HVC of all the forbidden lines studied here ([OI] $\lambda 6300$, [NII] $\lambda 6583$, [SII] $\lambda 6716$, [SII] $\lambda 6731$). These are listed in tables D.1, D.2, D.3, D.4, D.5, D.6, D.7.

Appendix E: Additional information on targets

Table E.1 lists the additional information on targets used in this work (Maucó et al. 2023, 2016). Typical uncertainties on A_V , L_* , M_* , L_{acc} , \dot{M}_{acc} are 0.1 mag, 0.2 dex, 0.1 dex, 0.25 dex, 0.45 dex, respectively (Manara et al. 2021).

Table A.1. Parameters for the [OI] $\lambda 6300$ LVC for the X-shooter sample

Name	$\log L_{\text{OI,LVC}}^1$ [L_{\odot}]	FWHM ² [km/s]	v_{peak}^2 [km/s]	EW [Å]	F_{cont} [erg s ⁻¹ nm ⁻¹ cm ⁻²]	$\log L_{\text{OI,GC}}^3$ [L_{\odot}]	Class ⁴
SO73	-4.93	36.6	-12.03	0.42	2.66e-14	-5.34	LVC-NC
SO73		164.8	-24.61	0.71	2.66e-14	-5.12	LVC-BC
SO299	-6.12	41.9	6.96	0.18	1.08e-14	-6.12	LVC-SC
SO341	-4.1	80.9	-14.23	2.06	7.41e-14	-4.1	LVC-SC
SO362	-4.75	126.8	-13.51	0.64	5.44e-14	-4.75	LVC-SC
SO467	-6.27	99.9	2.44	0.93	1.20e-15	-6.27	LVC-SC
SO490	-6.41	79.5	-15.57	0.52	1.50e-15	-6.41	LVC-SC
SO500	-6.87	98.4	-11.09	0.99	3.00e-16	-6.87	LVC-SC
SO518	-4.43	162.2	10.24	0.63	1.17e-13	-4.43	LVC-BC
SO520	-6.33	81.6	-3.3	0.15	6.30e-15	-6.33	LVC-SC
SO540	-4.58	47.3	-2.01	0.55	9.22e-14	-4.58	LVC-SC
SO562	-5.49	43.6	-7.16	0.53	1.22e-14	-5.49	LVC-SC
SO563	-5.18	75.9	-15.93	0.29	4.48e-14	-5.18	LVC-SC
SO583	-4.3	72.8	-11.82	0.12	8.46e-13	-4.3	LVC-SC
SO587	-5.13	57.7	-4.33	1.2	1.23e-14	-5.13	LVC-SC
SO646	-5.57	70.6	-0.39	0.75	7.10e-15	-5.57	LVC-SC
SO662	-4.98	56.8	-6.07	0.25	8.20e-14	-4.98	LVC-SC
SO687	-5.78	23.5	5.49	0.05	6.17e-14	-5.78	LVC-NC
SO694	-6.18	30.7	-10.27	0.46	3.00e-15	-6.18	LVC-SC
SO697	-5.28	44.3	-6.12	0.07	1.57e-13	-5.28	LVC-SC
SO726	-4.7	147.9	-6.0	0.66	5.88e-14	-4.7	LVC-SC
SO774	-5.3	57.7	3.13	0.36	2.76e-14	-5.3	LVC-SC
SO818	-5.0	72.2	-4.98	0.59	3.29e-14	-5.0	LVC-SC
SO823	-4.44	80.4	-3.36	1.9	3.79e-14	-4.44	LVC-SC
SO844	-5.25	73.2	-29.26	0.57	1.82e-14	-5.25	LVC-SC
SO848	-5.47	75.7	-24.02	6.27	1.10e-15	-5.55	LVC-BC
SO848		29.9	4.27	1.16	1.10e-15	-6.29	LVC-NC
SO859	-5.36	46.4	5.19	0.49	1.70e-14	-5.36	LVC-BC
SO897	-4.69	69.9	4.32	0.29	1.39e-13	-4.69	LVC-SC
SO927	-5.07	68.4	-3.12	0.45	3.57e-14	-5.07	LVC-BC
SO1036	-4.93	50.1	0.71	0.28	8.73e-14	-4.93	LVC-BC
SO1152	-5.07	72.4	3.4	0.21	8.03e-14	-5.07	LVC-SC
SO1153	-3.88	58.2	-19.09	1.44	1.86e-13	-3.88	LVC-BC
SO1154	-4.81	101.7	6.74	1.48	2.09e-14	-4.81	LVC-BC
SO1156	-4.77	38.9	2.38	0.3	1.13e-13	-4.77	LVC-NC
SO1260	-5.73	40.8	2.35	0.47	8.50e-15	-5.73	LVC-BC
SO1266	-6.03	49.7	4.73	0.77	2.40e-15	-6.03	LVC-SC
SO1274	-4.99	56.9	-0.05	0.18	1.05e-13	-4.99	LVC-SC
SO1327	-5.86	69.1	-0.07	0.29	9.50e-15	-5.86	LVC-SC
SO1361	-5.16	46.5	-2.66	0.14	9.66e-14	-5.16	LVC-BC
SO1362	-6.11	56.9	-7.88	0.93	1.70e-15	-6.11	LVC-SC
SO1369	-4.89	90.4	-11.34	0.16	1.61e-13	-4.89	LVC-SC

¹ Total LVC luminosity.² Median uncertainties. SC: $\delta_{v_{\text{peak}}} = 0.6$, $\delta_{\text{FWHM}} = 1.4$. NC: $\delta_{v_{\text{peak}}} = 0.3$, $\delta_{\text{FWHM}} = 0.9$. BC: $\delta_{v_{\text{peak}}} = 4.3$, $\delta_{\text{FWHM}} = 3.3$.³ Luminosity of each Gaussian component.⁴ LVC: Low-velocity component. SC: single-component. NC: narrow-component. BC: broad-component.

Table C.1. Parameters for the [NII] $\lambda 6583$ line LVC for the MIKE sample

Name	$\log L_{\text{NII,LVC}}^1$ [L_{\odot}]	FWHM ² [km/s]	v_{peak}^2 [km/s]	EW [Å]	F_{cont} [erg s ⁻¹ nm ⁻¹ cm ⁻²]	$\log L_{\text{NII,GC}}^3$ [L_{\odot}]	Class
SO341	-5.34	27.1	-5.43	0.1	8.66e-14	-5.34	LVC-NC
SO396	-5.12	15.4	1.05	0.18	8.66e-14	-5.12	LVC-SC
SO518	-6.66	17.8	-7.73	0.0	1.26e-13	-6.66	LVC-NC
SO562	-4.83	60.1	-18.13	0.4	1.99e-14	-5.4	LVC-BC
SO562		19.6	-5.34	1.03	1.99e-14	-4.99	LVC-NC
SO583	-4.65	46.1	-1.49	0.05	8.81e-13	-4.65	LVC-SC
SO615	-4.64	60.8	14.98	0.05	8.81e-13	-4.64	LVC-SC
SO638	-5.82	14.9	23.03	0.0	8.81e-13	-5.82	LVC-NC
SO662	-4.77	40.8	-1.11	0.36	9.44e-14	-4.77	LVC-SC
SO682	-5.44	26.9	4.59	0.07	9.61e-14	-5.44	LVC-SC
SO687	-4.5	22.9	-0.75	0.52	7.89e-14	-4.66	LVC-NC
SO687		13.3	11.58	0.22	7.89e-14	-5.03	LVC-NC
SO859	-5.89	21.8	3.3	0.1	2.59e-14	-5.89	LVC-SC
SO897	-4.86	22.1	-0.75	0.18	1.49e-13	-4.86	LVC-SC
SO927	-6.8	31.1	3.77	0.01	4.25e-14	-6.8	LVC-NC
SO984	-7.01	19.6	1.53	0.0	9.82e-14	-7.01	LVC-NC
SO1036	-4.78	18.2	-0.14	0.32	1.06e-13	-4.78	LVC-SC
SO1153	-6.69	11.8	-26.49	0.0	2.23e-13	-6.69	LVC-NC
SO1361	-5.43	11.8	-4.99	0.06	1.17e-13	-5.43	LVC-NC

¹ Total LVC luminosity.² Median uncertainties. SC: $\delta_{v_{\text{peak}}} = 3.0$, $\delta_{\text{FWHM}} = 4.5$. NC: $\delta_{v_{\text{peak}}} = 1.9$, $\delta_{\text{FWHM}} = 2.3$. BC: $\delta_{v_{\text{peak}}} = 4.6$, $\delta_{\text{FWHM}} = 7.2$.³ Luminosity of each Gaussian component.**Table C.2.** Parameters for the [SII] $\lambda 6731$ LVC for the MIKE sample

Name	$\log L_{\text{SII,LVC}}^1$ [L_{\odot}]	FWHM ² [km/s]	v_{peak}^2 [km/s]	EW [Å]	F_{cont} [erg s ⁻¹ nm ⁻¹ cm ⁻²]	$\log L_{\text{SII,GC}}^3$ [L_{\odot}]	Class
SO341	-4.74	42.4	-25.52	0.46	7.61e-14	-4.74	LVC-BC
SO396	-5.01	15.4	-5.8	0.26	7.61e-14	-5.01	LVC-SC
SO662	-5.41	33.7	-7.86	0.09	8.55e-14	-5.41	LVC-NC
SO1036	-5.58	16.7	-6.7	0.06	9.08e-14	-5.58	LVC-SC

¹ Total LVC luminosity.² Median uncertainties. SC: $\delta_{v_{\text{peak}}} = 1.3$, $\delta_{\text{FWHM}} = 1.8$. NC: $\delta_{v_{\text{peak}}} = 1.3$, $\delta_{\text{FWHM}} = 1.9$. BC: $\delta_{v_{\text{peak}}} = 0.8$, $\delta_{\text{FWHM}} = 0.9$.³ Luminosity of each Gaussian component.**Table C.3.** Parameters for the [SII] $\lambda 6716$ LVC for the MIKE sample

Name	$\log L_{\text{SII,LVC}}^1$ [L_{\odot}]	FWHM ² [km/s]	v_{peak}^2 [km/s]	EW [Å]	F_{cont} [erg s ⁻¹ nm ⁻¹ cm ⁻²]	$\log L_{\text{SII,GC}}^3$ [L_{\odot}]	Class
SO341	-4.98	37.7	2.79	0.41	7.61e-14	-4.98	LVC-NC
SO396	-4.73	15.4	21.79	0.21	7.61e-14	-4.73	LVC-SC
SO1036	-5.94	12.3	20.54	0.02	9.08e-14	-5.94	LVC-SC

¹ Total LVC luminosity.² Median uncertainties. SC: $\delta_{v_{\text{peak}}} = 1.3$, $\delta_{\text{FWHM}} = 1.8$. NC: $\delta_{v_{\text{peak}}} = 1.3$, $\delta_{\text{FWHM}} = 1.9$. BC: $\delta_{v_{\text{peak}}} = 0.8$, $\delta_{\text{FWHM}} = 0.9$.³ Luminosity of each Gaussian component.

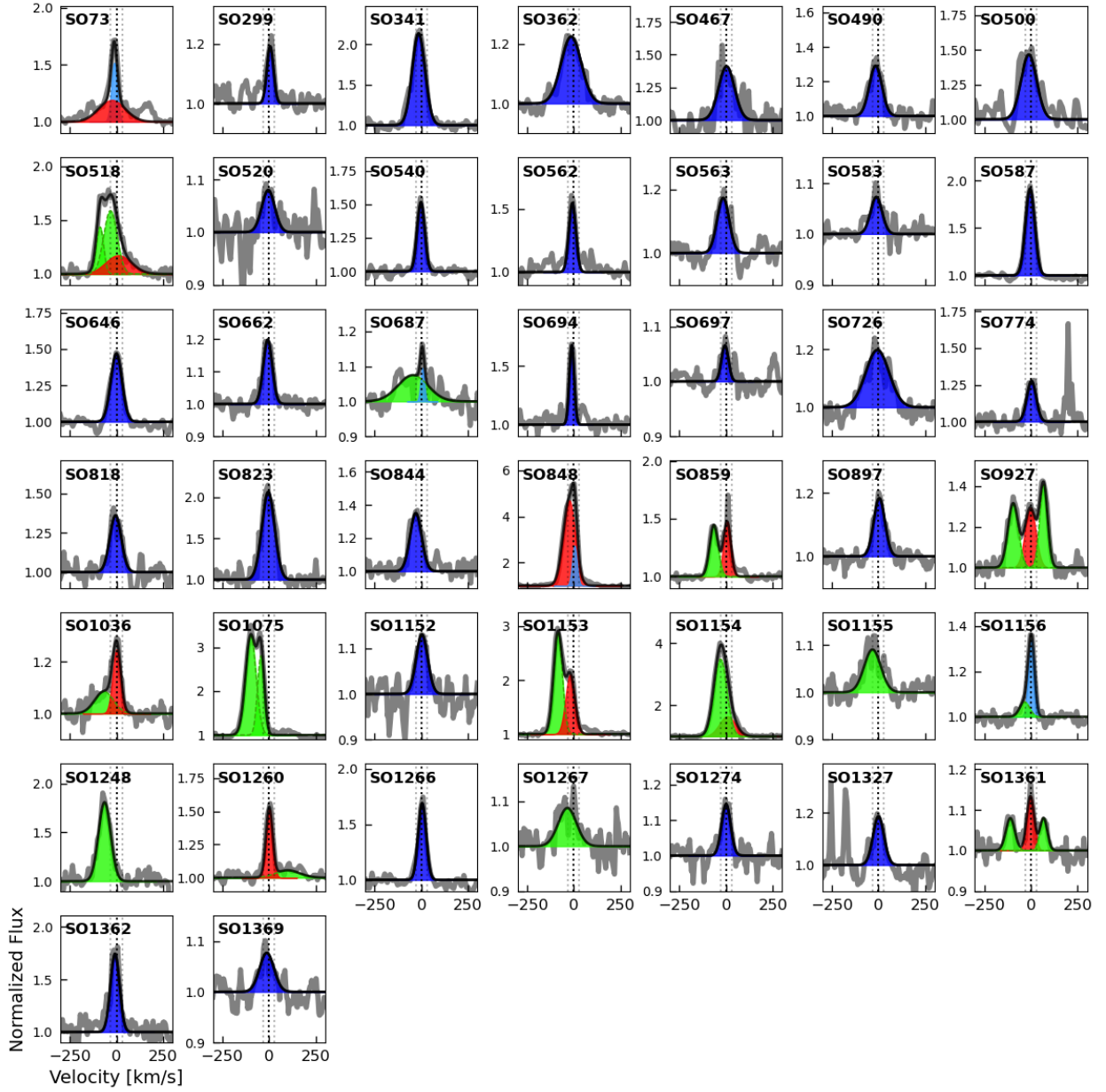


Fig. A.1. [OI] $\lambda 6300$ lines fit for the X-shooter sample. The colors indicate the type of Gaussian component as described in Fig. 3. The black dotted line is located at 0 km/s, while the gray dotted lines indicate the velocity threshold for the high/low-velocity component (± 30 km/s).

Table C.4. Parameters for the [NII] $\lambda 6583$ LVC for the X-shooter sample

Name	$\log L_{\text{NII,LVC}}^1$ [L_{\odot}]	FWHM ² [km/s]	v_{peak}^2 [km/s]	EW [Å]	F_{cont} [erg s ⁻¹ nm ⁻¹ cm ⁻²]	$\log L_{\text{NII,GC}}^3$ [L_{\odot}]	Class
SO341	-4.99	91.6	-29.56	0.23	8.66e-14	-4.99	LVC-SC
SO518	-5.33	23.5	2.1	0.07	1.27e-13	-5.33	LVC-NC
SO583	-4.59	54.9	10.0	0.06	8.81e-13	-4.59	LVC-SC
SO587	-4.69	46.0	1.87	2.17	1.87e-14	-4.69	LVC-SC
SO662	-4.66	45.6	-2.4	0.45	9.44e-14	-4.66	LVC-SC
SO682	-5.28	53.1	0.3	0.1	9.61e-14	-5.28	LVC-SC
SO687	-4.57	36.6	1.1	0.64	7.89e-14	-4.57	LVC-SC
SO694	-5.25	34.3	-0.76	2.23	5.20e-15	-5.25	LVC-SC
SO726	-4.59	58.0	1.76	0.7	7.20e-14	-4.59	LVC-SC
SO823	-5.7	25.1	-7.55	0.1	4.19e-14	-5.7	LVC-SC
SO848	-5.25	39.5	-0.06	8.0	1.80e-15	-5.25	LVC-NC
SO859	-5.82	35.4	2.98	0.11	2.59e-14	-5.82	LVC-NC
SO897	-4.92	27.6	-0.63	0.16	1.49e-13	-4.92	LVC-SC
SO927	-5.33	33.3	2.97	0.2	4.25e-14	-5.33	LVC-NC
SO1036	-4.6	22.4	-3.08	0.49	1.06e-13	-4.6	LVC-SC
SO1075	-4.43	35.9	-13.37	4.09	1.92e-14	-4.43	LVC-SC
SO1154	-5.04	70.6	-23.51	0.76	2.39e-14	-5.04	LVC-BC
SO1260	-6.28	62.6	6.19	0.09	1.22e-14	-6.28	LVC-BC
SO1267	-6.0	23.5	7.94	0.03	6.56e-14	-6.0	LVC-SC

¹ Total LVC luminosity.² Median uncertainties. SC: $\delta_{v_{\text{peak}}} = 5.2$, $\delta_{\text{FWHM}} = 3.5$. NC: $\delta_{v_{\text{peak}}} = 3.6$, $\delta_{\text{FWHM}} = 2.2$. BC: $\delta_{v_{\text{peak}}} = 5.5$, $\delta_{\text{FWHM}} = 6.5$.³ Luminosity of each Gaussian component.**Table C.5.** Parameters for the [SII] $\lambda 6731$ LVC for the X-shooter sample

Name	$\log L_{\text{SII,LVC}}^1$ [L_{\odot}]	FWHM ² [km/s]	v_{peak}^2 [km/s]	EW [Å]	F_{cont} [erg s ⁻¹ nm ⁻¹ cm ⁻²]	$\log L_{\text{SII,GC}}^3$ [L_{\odot}]	Class
SO500	-7.48	68.0	-24.59	0.19	3.00e-16	-7.48	LVC-SC
SO563	-5.53	117.5	-10.92	0.12	4.72e-14	-5.53	LVC-SC
SO583	-4.88	47.1	-1.64	0.03	8.32e-13	-4.88	LVC-BC
SO587	-4.96	49.6	-17.72	1.59	1.37e-14	-4.96	LVC-SC
SO662	-5.32	48.3	-3.8	0.11	8.55e-14	-5.32	LVC-SC
SO697	-5.65	40.1	-1.15	0.03	1.59e-13	-5.65	LVC-SC
SO848	-5.82	56.9	-17.63	2.98	1.30e-15	-5.82	LVC-BC
SO1036	-5.37	19.3	-7.08	0.1	9.08e-14	-5.37	LVC-SC
SO1155	-5.05	43.1	-11.76	0.06	3.00e-13	-5.05	LVC-SC
SO1260	-6.38	64.6	21.75	0.1	9.10e-15	-6.38	LVC-BC
SO1266	-6.52	28.1	-6.64	0.21	2.80e-15	-6.52	LVC-SC

¹ Total LVC luminosity.² Median uncertainties. SC: $\delta_{v_{\text{peak}}} = 6.8$, $\delta_{\text{FWHM}} = 8.7$. BC: $\delta_{v_{\text{peak}}} = 4.5$, $\delta_{\text{FWHM}} = 5.0$.³ Luminosity of each Gaussian component.

Table C.6. Parameters for the [SII] $\lambda 6716$ LVC for the X-shooter sample

Name	$\log L_{\text{SII,LVC}}^1$ [L_{\odot}]	FWHM ² [km/s]	v_{peak}^2 [km/s]	EW [Å]	F_{cont} [erg s ⁻¹ nm ⁻¹ cm ⁻²]	$\log L_{\text{SII,GC}}^3$ [L_{\odot}]	Class
SO587	-5.15	53.8	3.84	1.03	1.37e-14	-5.15	LVC-SC
SO848	-5.70	85.39	-9.07	4.00	1.30e-15	-5.70	LVC-SC
SO1266	-6.56	33.67	2.32	0.19	2.80e-15	-6.56	LVC-SC

¹ Total LVC luminosity.² Median uncertainties. SC: $\delta_{v_{\text{peak}}} = 6.8$, $\delta_{\text{FWHM}} = 8.7$. BC: $\delta_{v_{\text{peak}}} = 4.5$, $\delta_{\text{FWHM}} = 5.0$.³ Luminosity of each Gaussian component.

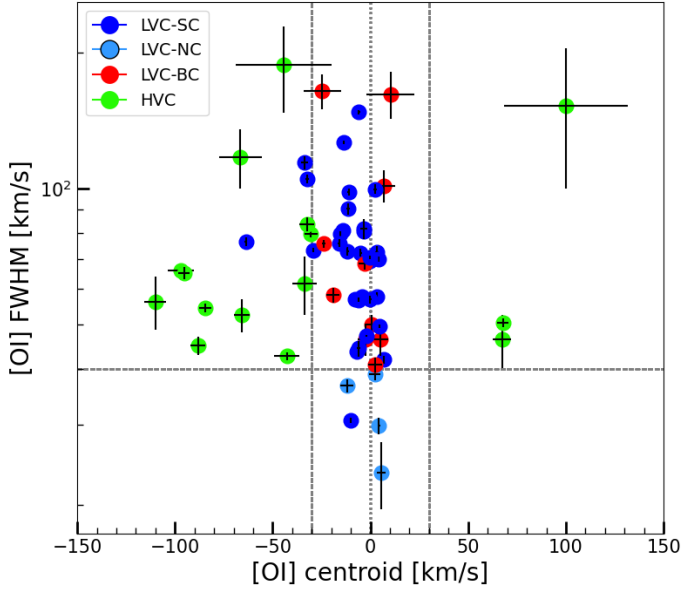


Fig. A.2. Kinematics of the [OI] $\lambda 6300$: FWHM vs v_{peak} , for σ -Orionis sources for the X-shooter sample. Colors indicate the type of Gaussian component as described in Fig. 3. Vertical lines indicate the systemic stellar velocity (0 km/s) and the velocity limit between low and high-velocity components (± 30 km/s). The horizontal line indicates the width threshold assumed for the broad and narrow components (40 km/s).

Table D.1. Kinematics properties of the [OI] $\lambda 6300$ HVC for the MIKE sample

Name	v_{peak} [km/s]	FWHM [km/s]
SO362	32.1 ± 1.1	26.6 ± 0.1
SO518	-102.1 ± 0.8	49.5 ± 0.1
SO518	-37.4 ± 0.8	74.7 ± 0.0
SO844	-60.6 ± 1.2	33.4 ± 1.5
SO859	-69.2 ± 1.8	28.0 ± 0.1
SO927	-93.9 ± 0.8	121.9 ± 0.1
SO927	75.1 ± 0.8	69.3 ± 0.0
SO1036	-91.2 ± 12.2	92.4 ± 20.3
SO1153	-97.3 ± 0.8	33.1 ± 0.0
SO1153	-69.3 ± 0.8	106.3 ± 0.0
SO1361	-119.0 ± 3.2	30.2 ± 5.2
SO1361	-31.1 ± 9.1	157.1 ± 15.1
SO1361	86.7 ± 2.5	22.6 ± 4.0

Table D.2. Kinematics properties of the [OI] $\lambda 6300$ HVC for the X-shooter sample

Name	v_{peak} [km/s]	FWHM [km/s]
SO518	-32.5 ± 3.9	83.6 ± 3.0
SO518	-88.3 ± 3.7	45.0 ± 2.2
SO687	-44.6 ± 24.5	188.4 ± 40.9
SO859	-65.7 ± 4.0	52.6 ± 4.5
SO927	-95.4 ± 3.0	65.2 ± 2.0
SO927	67.8 ± 2.8	50.6 ± 1.2
SO1036	-66.5 ± 10.9	117.7 ± 17.6
SO1075	-96.9 ± 6.6	66.1 ± 1.0
SO1075	-42.8 ± 6.6	42.6 ± 0.8
SO1153	-84.6 ± 3.1	54.6 ± 1.2
SO1154	-30.4 ± 3.3	79.7 ± 1.7
SO1156	-33.6 ± 6.1	61.8 ± 9.1
SO1260	100.0 ± 31.7	152.6 ± 52.5
SO1361	-110.1 ± 5.4	56.3 ± 7.6
SO1361	67.4 ± 4.7	46.4 ± 6.2

Table D.3. Kinematics properties of the [NII] $\lambda 6583$ HVC for the MIKE sample

Name	v_{peak} [km/s]	FWHM [km/s]
SO341	-69.0 ± 3.6	60.4 ± 6.0
SO518	-98.8 ± 17.8	56.2 ± 29.6
SO638	38.3 ± 19.0	62.7 ± 31.6
SO927	69.9 ± 16.1	65.0 ± 26.8
SO984	-56.0 ± 11.1	64.3 ± 18.3
SO1153	-94.5 ± 4.5	36.5 ± 7.4
SO1361	80.8 ± 4.1	35.9 ± 6.8

Table D.4. Kinematics properties of the [NII] $\lambda 6583$ HVC for the X-shooter sample

Name	v_{peak} [km/s]	FWHM [km/s]
SO73	148.9 ± 4.8	58.7 ± 8.0
SO467	30.7 ± 7.7	51.9 ± 11.1
SO518	-70.2 ± 5.2	50.1 ± 6.3
SO540	35.3 ± 3.4	23.5 ± 3.4
SO562	-75.4 ± 0.5	36.5 ± 0.8
SO848	-43.0 ± 3.5	60.1 ± 1.8
SO859	-60.7 ± 11.6	61.8 ± 18.6
SO927	32.1 ± 8.0	110.1 ± 12.3
SO1154	60.0 ± 4.9	38.8 ± 5.9
SO1260	171.4 ± 7.8	54.8 ± 11.3

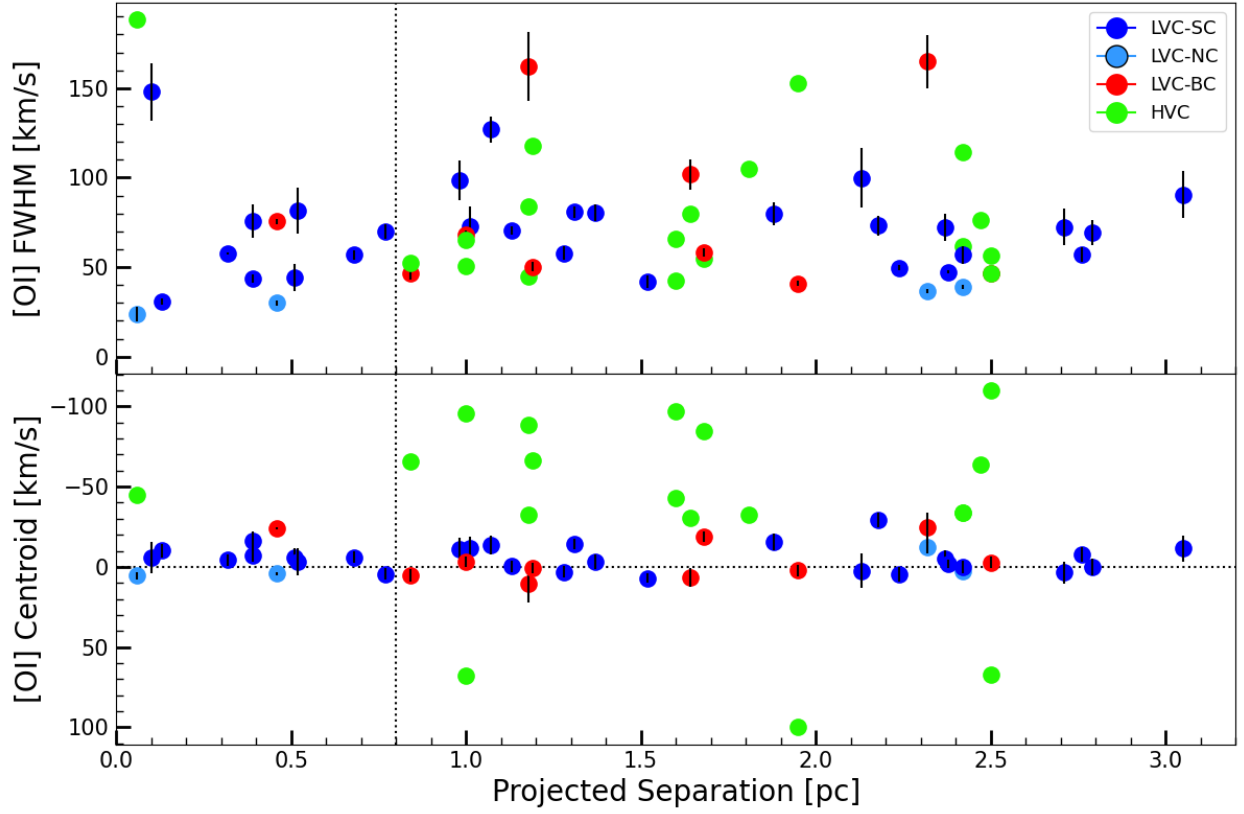


Fig. A.3. [OI] $\lambda 6300$ lines FWHM (top) and peak velocity (bottom) as a function of projected separation from σ -Ori for the X-shooter sample. The colors represent the type of Gaussian component as explained in sec 4.2. The vertical dotted line is positioned at 0.8 pc. The horizontal line indicates the systemic stellar velocity (0 km/s).

Table D.5. Kinematics properties of the [SII] $\lambda 6731$ HVC for the MIKE sample

Name	v_{peak} [km/s]	FWHM [km/s]
SO341	-72.0 ± 1.5	46.9 ± 2.4
SO518	-55.9 ± 19.1	61.5 ± 31.8
SO518	-100.0 ± 6.0	44.1 ± 10.0
SO662	63.4 ± 11.3	64.8 ± 18.8
SO844	-67.1 ± 2.0	21.4 ± 3.1
SO927	-109.8 ± 19.8	56.2 ± 33.0
SO927	67.6 ± 6.8	36.1 ± 11.2
SO927	47.4 ± 39.6	121.9 ± 66.0
SO1153	-61.8 ± 13.5	44.1 ± 22.4
SO1153	-100.0 ± 5.0	38.9 ± 8.3
SO1361	73.8 ± 1.9	27.2 ± 2.9
SO1361	-124.4 ± 2.7	28.4 ± 4.4

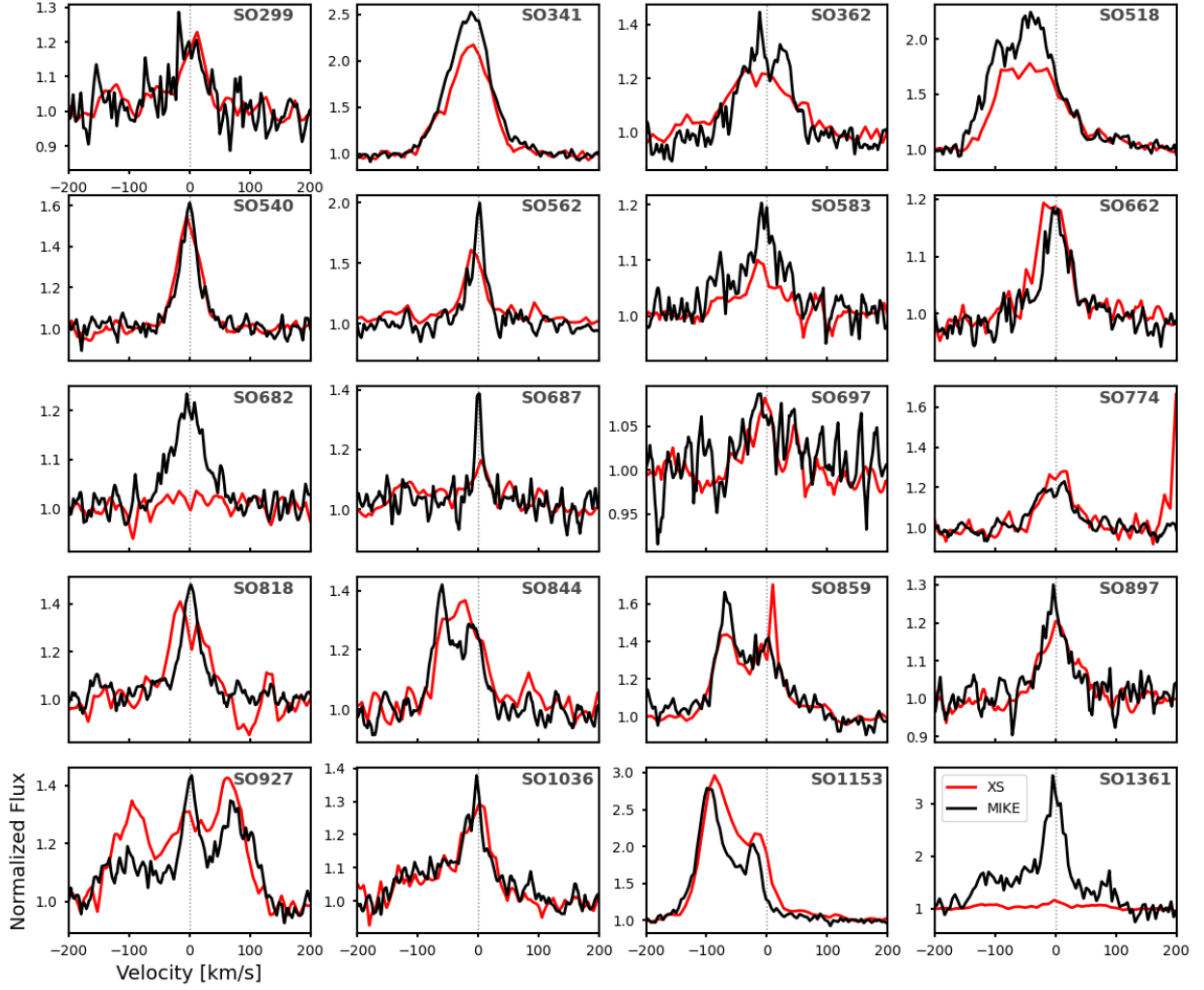


Fig. A.4. [OI] $\lambda 6300$ LVC line profiles comparison. MIKE spectra is shown in black while X-shooter (XS) spectra is shown in red. SO682 was not detected in X-shooter. SO1361 is detected in X-shooter but with a lower intensity than in MIKE spectra, as shown in Fig. A.1. The vertical dotted line indicates the systemic stellar velocity (0 km/s).

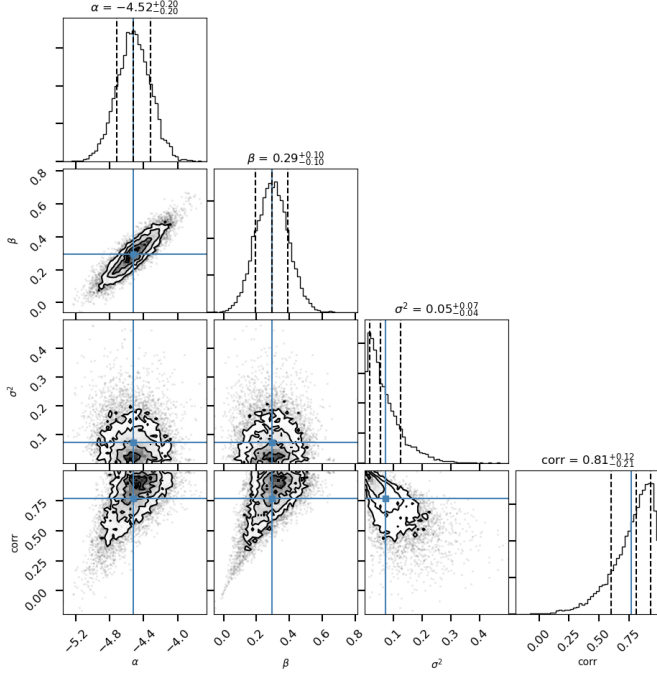


Fig. B.1. Corner plot of the $\log L_{\text{OLLVC}}$ vs. $\log L_{\text{acc}}$ fit for the complete sample, done using the linmix routine (Kelly 2007).

Table D.6. Kinematics properties of the [SII] $\lambda 6731$ HVC for the X-shooter sample

Name	v_{peak} [km/s]	FWHM [km/s]
SO73	67.0 ± 20.0	157.0 ± 32.8
SO73	156.0 ± 4.1	50.5 ± 3.9
SO341	-87.3 ± 3.3	40.4 ± 2.6
SO341	-32.0 ± 3.0	52.3 ± 1.4
SO518	-86.9 ± 3.7	27.9 ± 2.0
SO518	-66.1 ± 5.4	66.6 ± 7.0
SO583	115.1 ± 2.1	25.4 ± 3.6
SO726	-36.0 ± 7.3	93.0 ± 11.0
SO844	-66.7 ± 5.1	34.3 ± 6.9
SO848	-60.8 ± 3.6	48.4 ± 0.8
SO859	-76.8 ± 10.4	69.1 ± 16.6
SO927	-98.5 ± 5.5	65.8 ± 7.9
SO927	55.3 ± 4.2	61.4 ± 5.4
SO1075	-44.4 ± 6.6	39.2 ± 0.4
SO1075	-111.6 ± 6.6	57.9 ± 0.9
SO1153	-65.0 ± 3.4	71.1 ± 2.5
SO1153	-91.9 ± 3.1	36.2 ± 1.0
SO1154	34.7 ± 5.6	73.6 ± 7.6
SO1154	-45.3 ± 3.2	49.2 ± 1.1
SO1260	156.0 ± 7.8	97.6 ± 11.6
SO1362	305.8 ± 5.0	26.1 ± 2.4
SO1362	-93.2 ± 5.5	23.5 ± 4.6

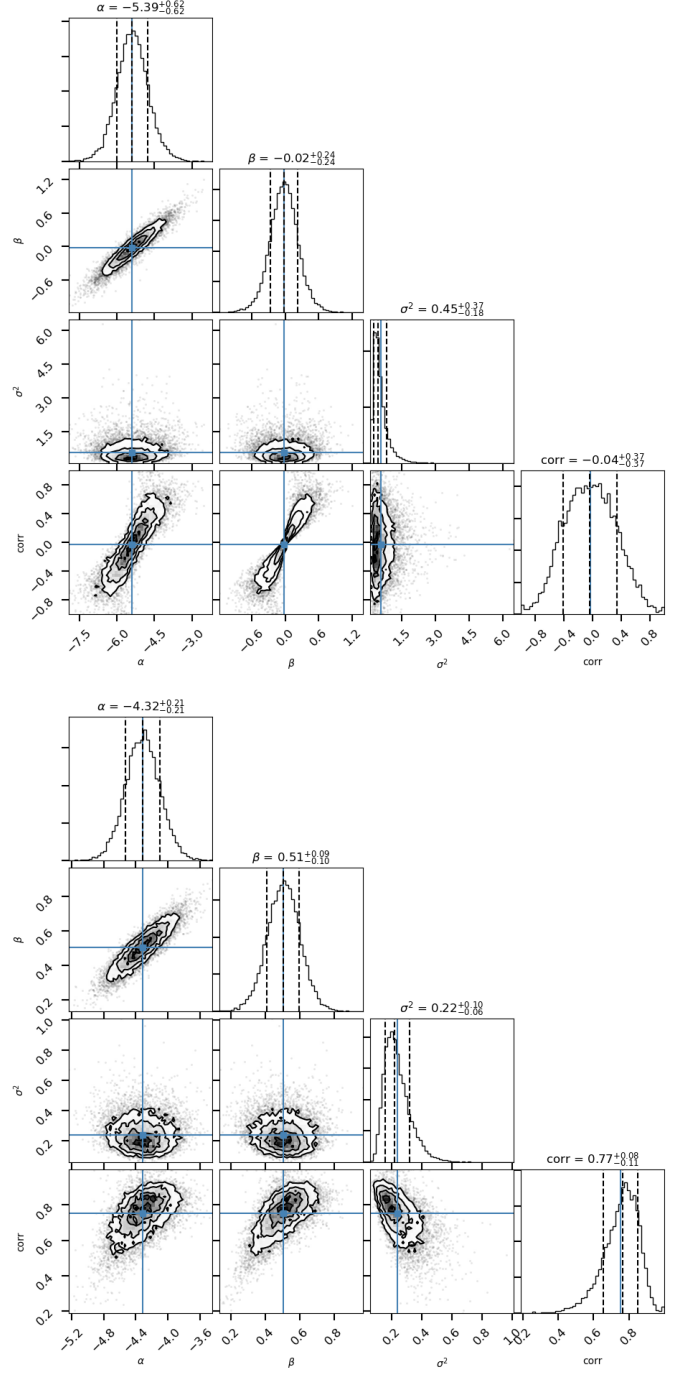


Fig. B.2. Corner plot of the $\log L_{\text{OLLVC}}$ vs. $\log L_{\text{acc}}$ fit for the near (top) and far (bottom) sample, done using the linmix routine (Kelly 2007).

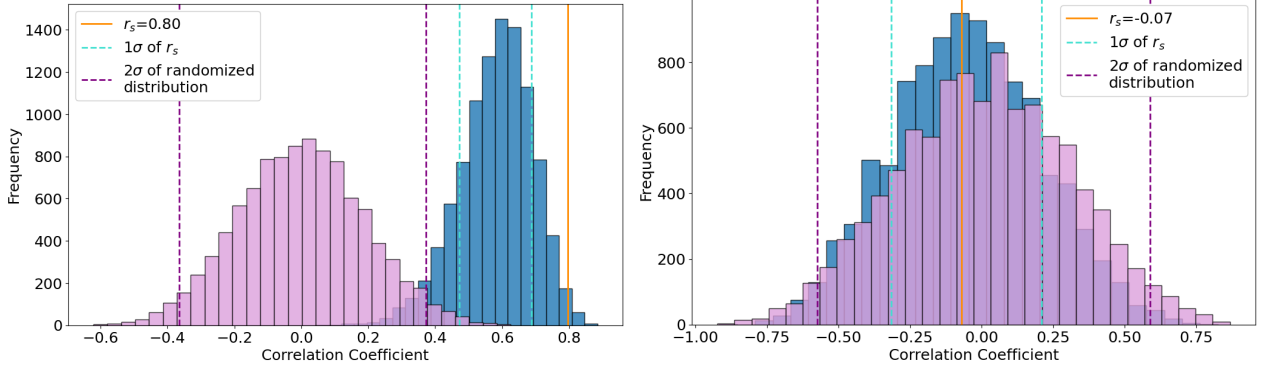


Fig. B.3. Correlation coefficient analysis for: sources beyond 0.8 pc (*left*) and within 0.8 pc (*right*). The violet histogram corresponds to the bootstrapped randomized x-axis values; the dashed purple lines mark the 2σ ranges of the realizations. The blue histogram results from bootstrapping the y-axis values within the respective error bars, and the 1σ ranges of the bootstrap are shown with cyan lines. We show that the Spearman correlation coefficient for the measured data (orange line), lies outside 2σ of the randomized distribution for the far sample and within 2σ for the near sample.

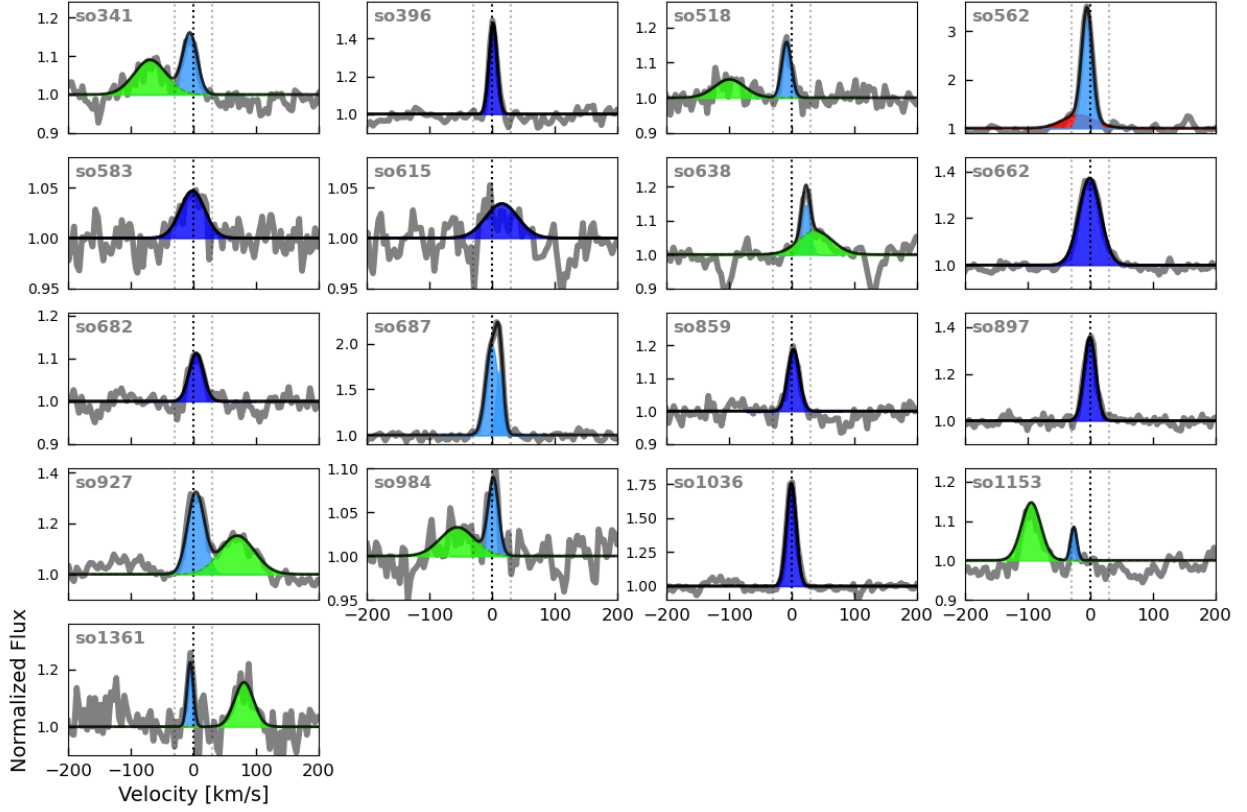


Fig. C.1. [NII] $\lambda 6583$ line fit profiles for the MIKE sample. The colors indicate the type of Gaussian component as described in sec 4.2. The black dotted line is located at 0 km/s, while the gray dotted lines indicate the velocity threshold for the high/low-velocity component (± 30 km/s).

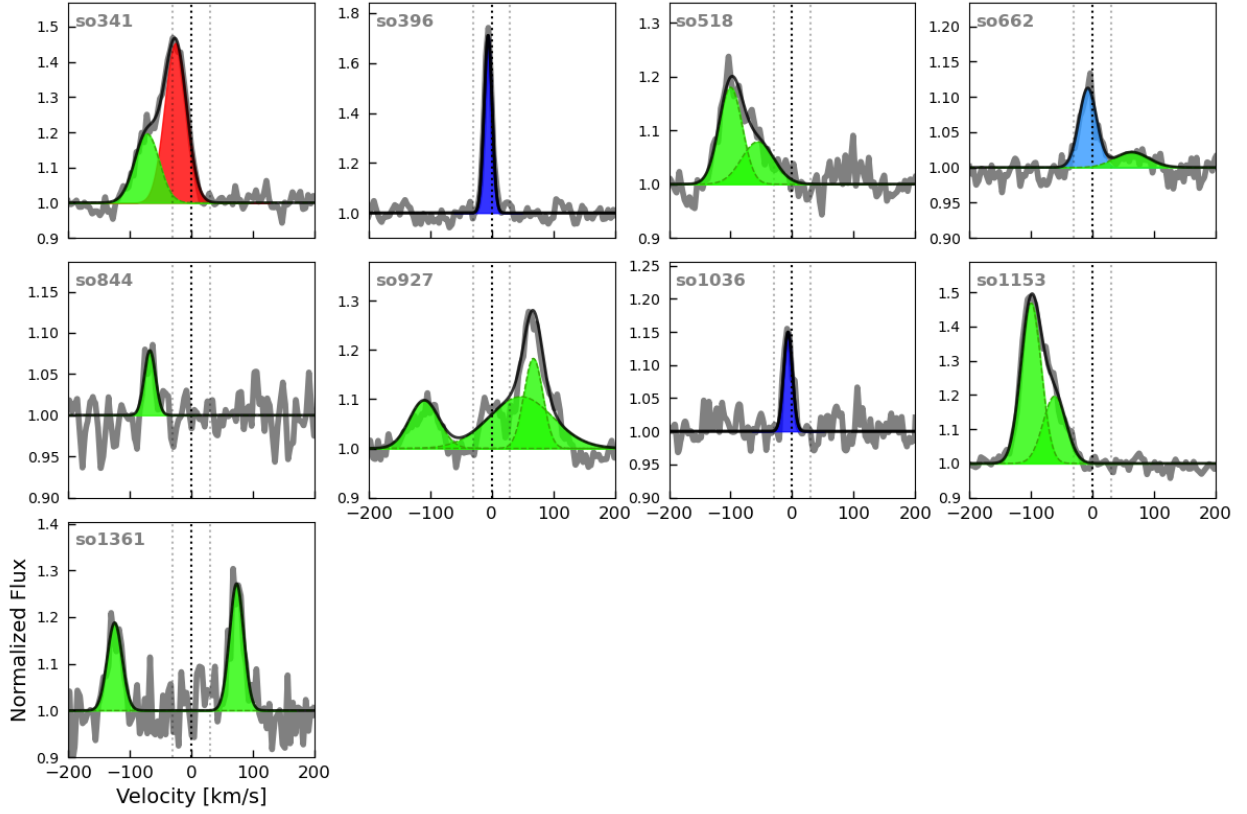


Fig. C.2. [SII] $\lambda 6731$ line fit profiles for the MIKE sample. The colors indicate the type of Gaussian component as described in sec 4.2. The black dotted line is located at 0 km/s, while the gray dotted lines indicate the velocity threshold for the high/low-velocity component (± 30 km/s).

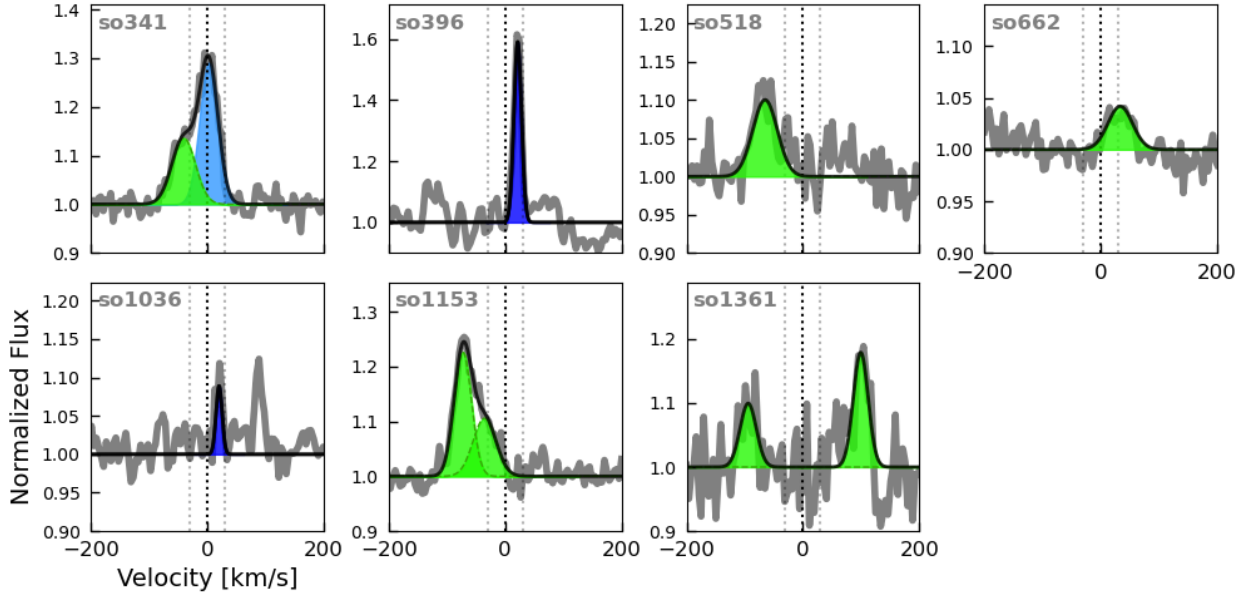


Fig. C.3. [SII] $\lambda 6716$ line fit profiles for the MIKE sample. The colors indicate the type of Gaussian component as described in sec 4.2. The black dotted line is located at 0 km/s, while the gray dotted lines indicate the velocity threshold for the high/low-velocity component (± 30 km/s).

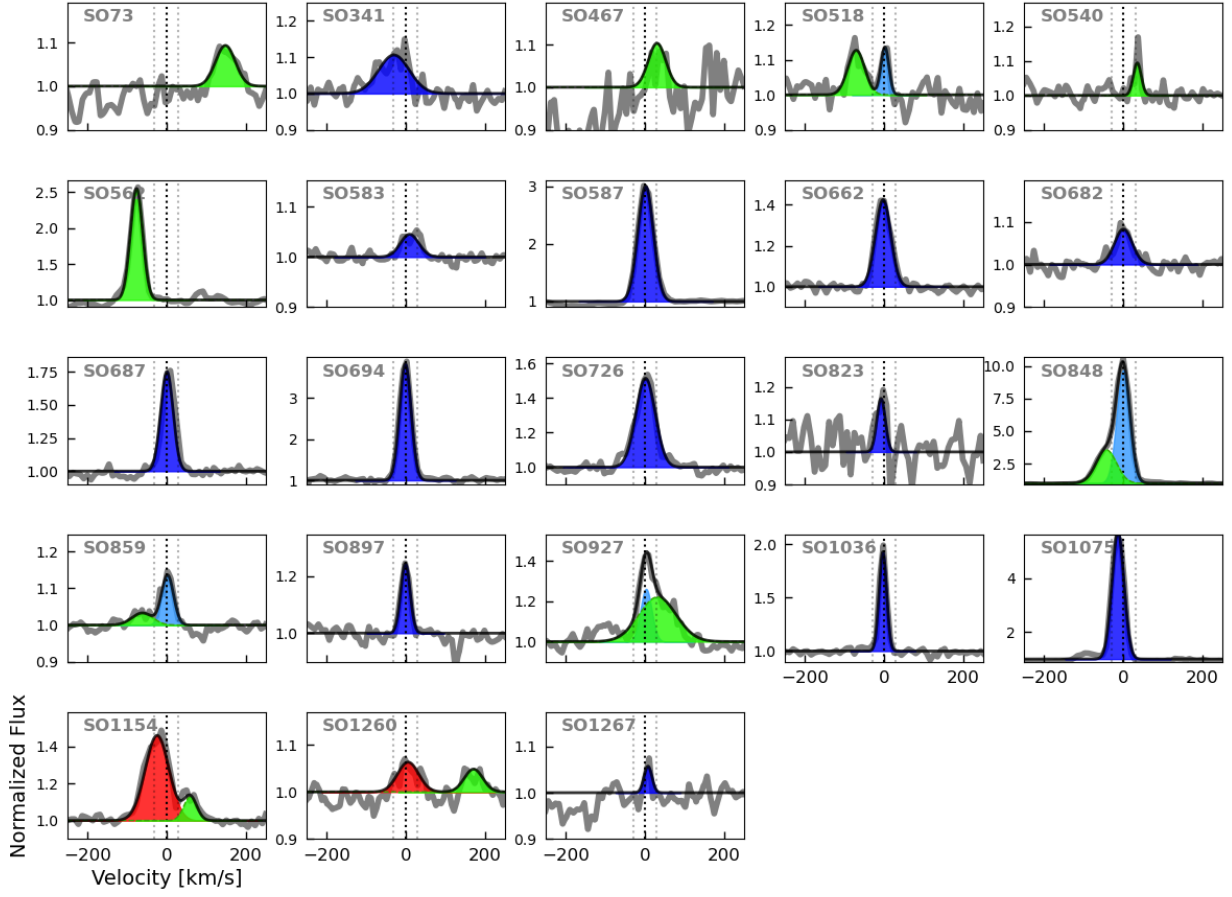


Fig. C.4. [NII] $\lambda 6583$ line fit profiles for the X-shooter sample. The colors indicate the type of Gaussian component as described in sec 4.2. The black dotted line is located at 0 km/s, while the gray dotted lines indicate the velocity threshold for the high/low-velocity component (± 30 km/s).

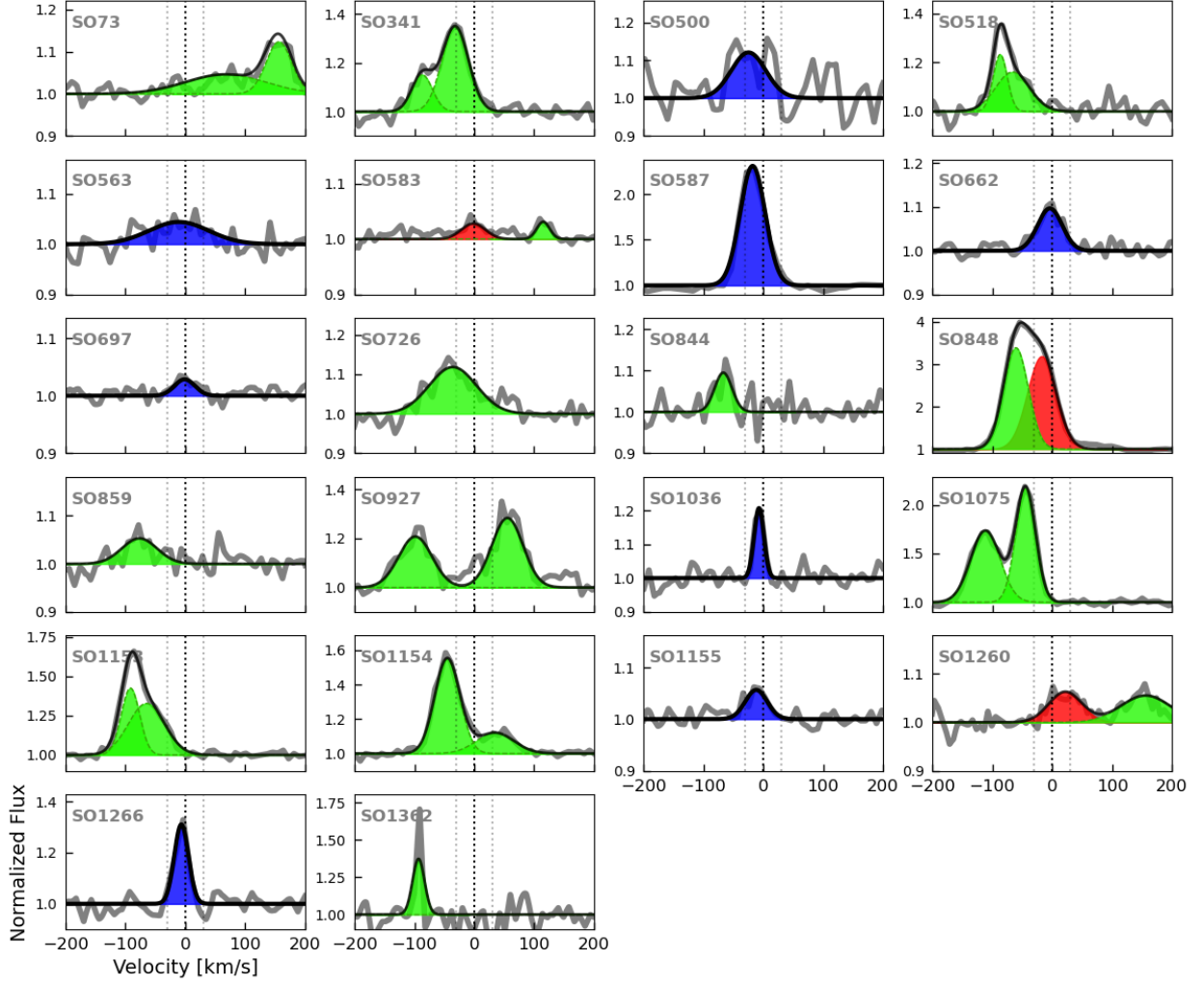


Fig. C.5. [SII] $\lambda 6731$ line fit profiles for the X-shooter sample. The colors indicate the type of Gaussian component as described in sec 4.2. The black dotted line is located at 0 km/s, while the gray dotted lines indicate the velocity threshold for the high/low-velocity component (± 30 km/s).

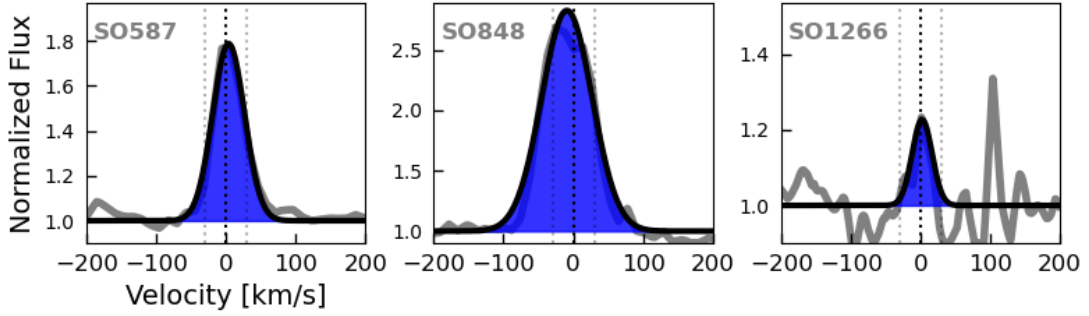


Fig. C.6. [SII] $\lambda 6716$ line fit profiles for the X-shooter sample. The colors indicate the type of Gaussian component as described in sec 4.2. The black dotted line is located at 0 km/s, while the gray dotted lines indicate the velocity threshold for the high/low-velocity component (± 30 km/s).

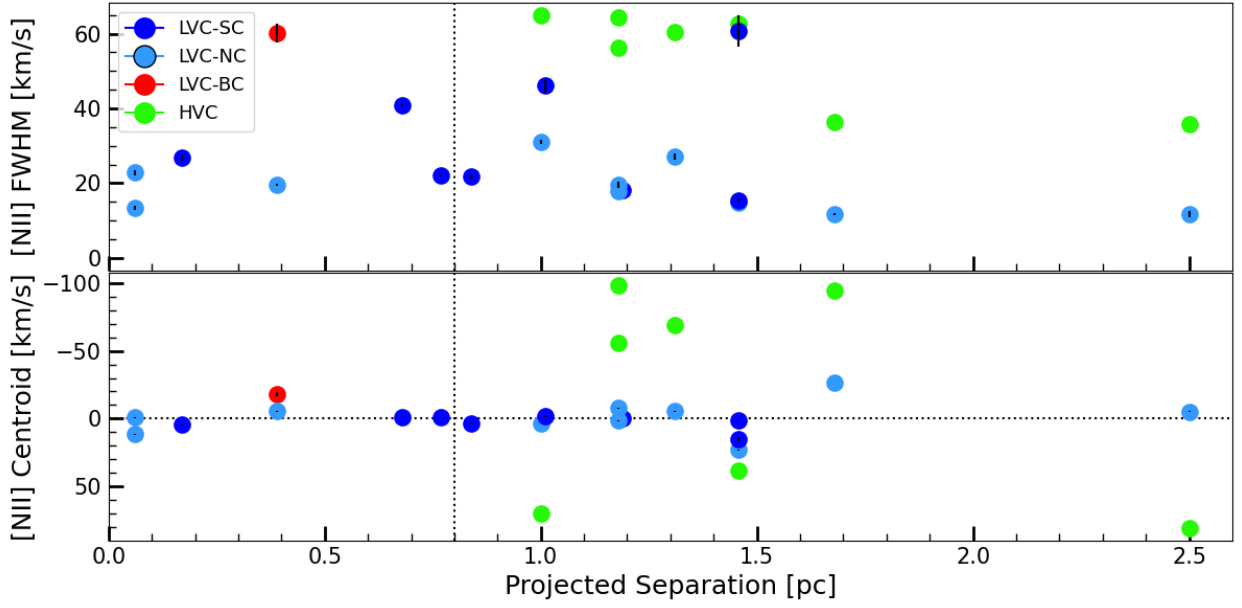


Fig. C.7. [NII] $\lambda 6583$ lines FWHM (top) and peak velocity (bottom) as a function of projected separation from σ -Ori for the MIKE sample. The colors represent the type of Gaussian component as explained in sec 4.2. The vertical dotted line is positioned at 0.8 pc. The horizontal line indicates the systemic stellar velocity (0 km/s).

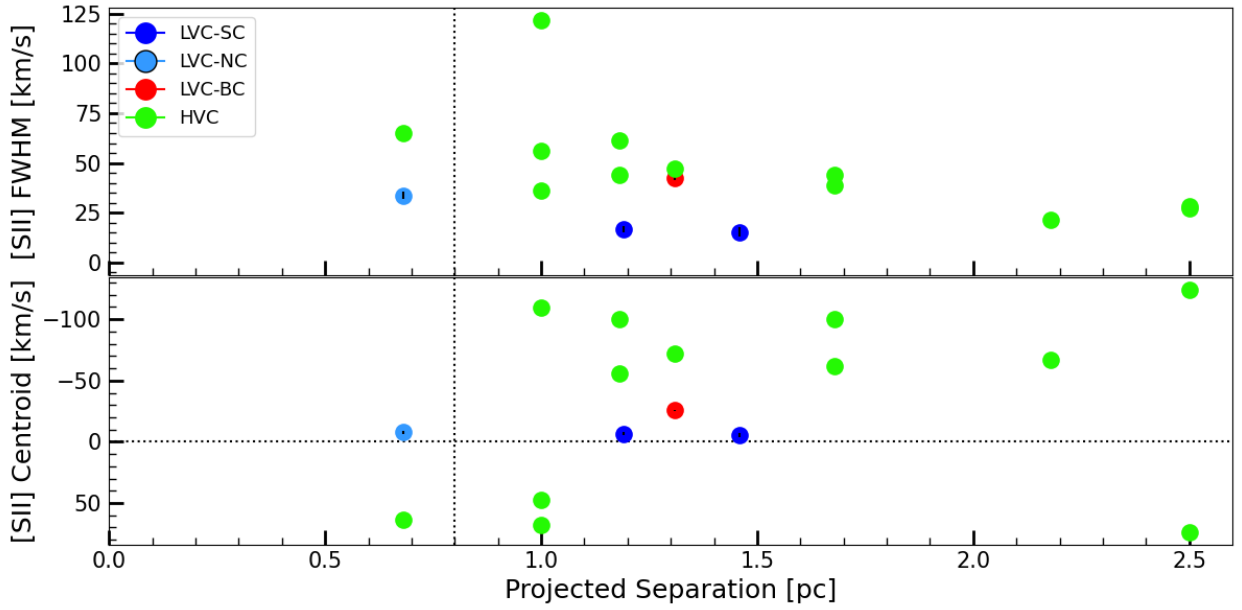


Fig. C.8. [SII] $\lambda 6731$ lines FWHM (top) and peak velocity (bottom) as a function of projected separation from σ -Ori for the MIKE sample. The colors represent the type of Gaussian component as explained in sec 4.2. The vertical dotted line is positioned at 0.8 pc. The horizontal line indicates the systemic stellar velocity (0 km/s).

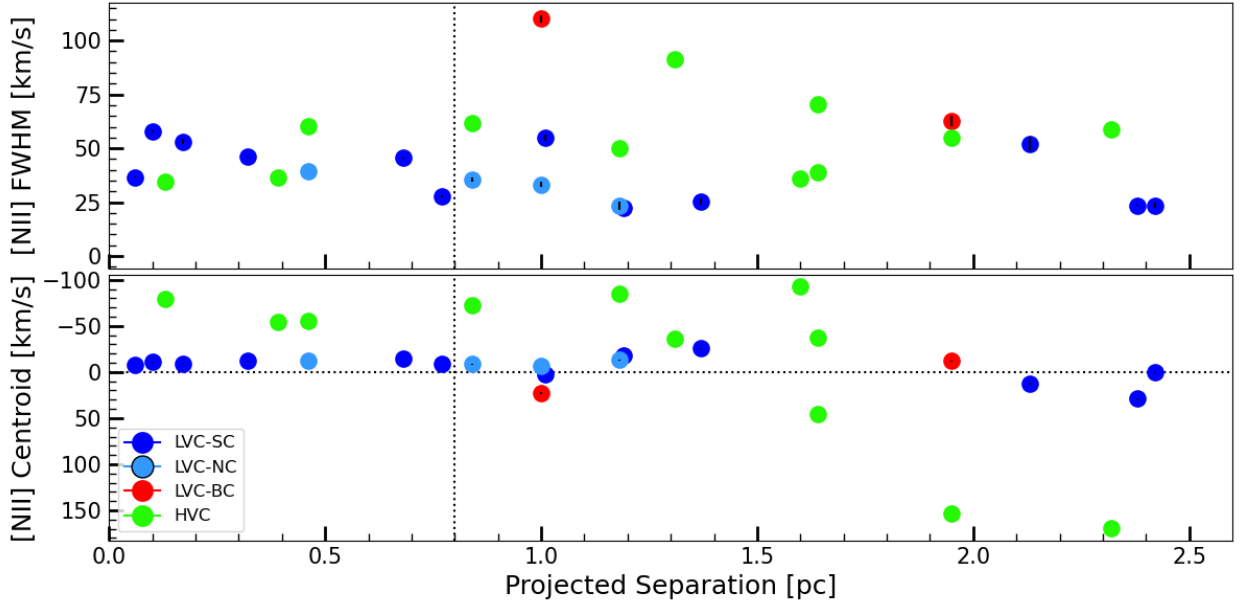


Fig. C.9. [NII] $\lambda 6583$ lines FWHM (top) and peak velocity (bottom) as a function of projected separation from σ -Ori for the X-shooter sample. The colors represent the type of Gaussian component as explained in sec 4.2. The vertical dotted line is positioned at 0.8 pc. The horizontal line indicates the systemic stellar velocity (0 km/s).

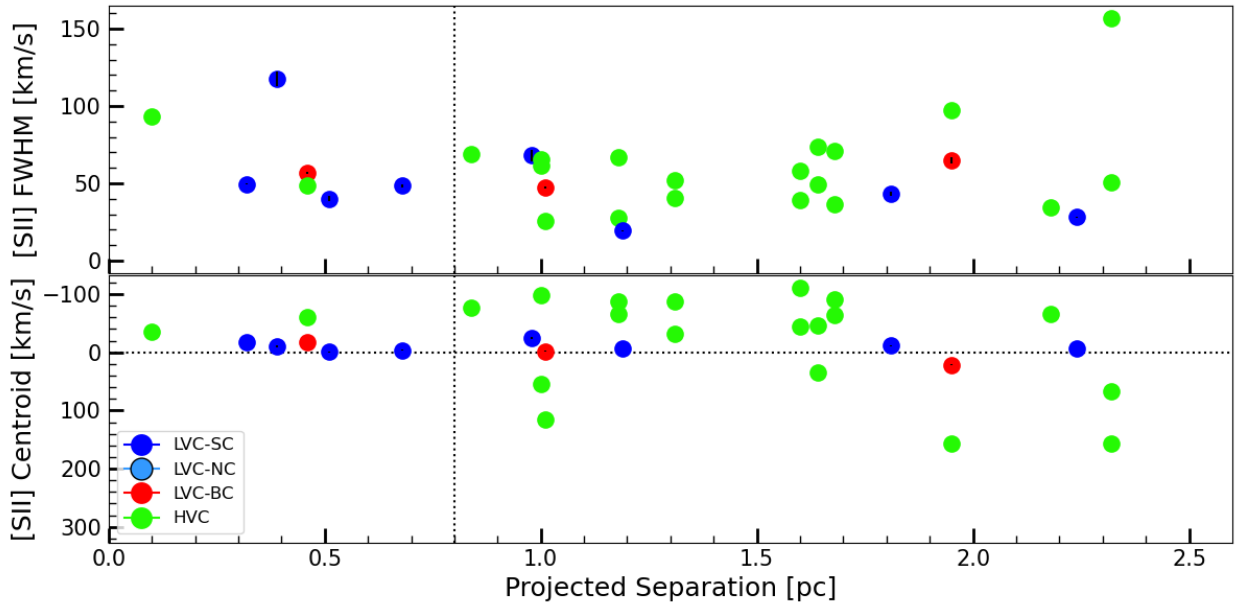


Fig. C.10. [SII] $\lambda 6731$ lines FWHM (top) and peak velocity (bottom) as a function of projected separation from σ -Ori for the X-shooter sample. The colors represent the type of Gaussian component as explained in sec 4.2. The vertical dotted line is positioned at 0.8 pc. The horizontal line indicates the systemic stellar velocity (0 km/s).

Table D.7. Kinematics properties of the [SII] $\lambda 6716$ HVC for the MIKE sample

Name	v_{peak} [km/s]	FWHM [km/s]
SO341	-40.4 ± 1.2	47.6 ± 2.2
SO518	-65.1 ± 0.8	49.9 ± 1.8
SO662	33.3 ± 0.7	49.6 ± 1.9
SO1153	-35.2 ± 2.2	46.4 ± 3.4
SO1153	-72.5 ± 0.7	35.3 ± 1.0
SO1361	99.3 ± 0.5	30.1 ± 1.3
SO1361	-94.1 ± 1.0	32.9 ± 2.5

Table E.1. Additional information on targets

Name	A _v [mag]	L _* [L _⊙]	logL _{acc} [L _⊙]	M _* [M _⊙]	log \dot{M}_{acc} [M _⊙ /yr]	Distance [pc]	dp [pc]	logG ₀	RV [km/s]
SO73	1.0	0.20	-1.13	0.29	-7.89	359.2 ^{+4.2} _{-4.4}	2.32	2.34	33.1
SO299	0.2	0.22	-2.62	0.24	-9.26	355.5 ^{+4.3} _{-4.4}	1.52	2.7	12.91
SO341	0.8	0.55	-1.18	0.59	-8.14	409.0 ^{+4.3} _{-4.4}	1.31	2.83	27.75
SO362	1.4	0.60	-0.7	0.3	-7.23	402.3 ^{+4.6} _{-4.8}	1.07	3.01	32.92
SO396	0.64	0.40	-1.20	0.42	-8.10	397.7 ^{+4.2} _{-4.2}	1.32	2.76	28.70
SO397	0.0	0.24	-2.62	0.19	-9.06	401.0	1.47	2.73	29.95
SO467	0.3	0.07	-3.18	0.1	-9.57	383.3 ^{+8.6} _{-9.0}	2.13	2.41	39.0
SO490	0.0	0.1	-3.01	0.13	-9.41	401.0	1.88	2.52	32.3
SO500	0.0	0.02	-3.84	0.06	-10.22	409.2 ^{+37.2} _{-45.4}	0.98	3.09	26.15
SO518	1.6	0.48	-0.69	0.8	-7.86	399.0 ^{+3.9} _{-4.0}	1.18	2.93	36.32
SO520	0.1	0.23	-2.01	0.18	-8.45	402.6 ^{+6.3} _{-6.5}	0.52	3.64	33.95
SO540	0.5	0.57	-1.84	0.77	-8.96	406.0 ^{+3.5} _{-3.6}	2.38	2.32	22.85
SO562	0.3	0.26	-1.44	0.15	-7.7	401.0	0.39	3.88	25.05
SO563	0.6	0.36	-1.27	0.64	-8.36	401.0	0.39	3.88	33.3
SO583	1.0	4.06	-0.69	1.18	-7.62	401.0	1.01	3.06	20.35
SO587	0.0	0.35	-3.91	0.21	-10.31	401.0	0.32	4.06	34.65
SO615	1.9	3.27	-1.92	1.49	-9.11	397.9 ^{+6.2} _{-6.2}	0.85	3.14	30.55
SO646	0.0	0.12	-2.9	0.25	-9.66	404.6 ^{+6.6} _{-6.8}	1.13	2.96	32.1
SO662	0.3	0.68	-3.79	0.64	-10.77	401.2 ^{+3.3} _{-3.4}	0.68	3.41	27.55
SO682	0.7	0.76	-2.02	0.57	-8.89	409.8 ^{+4.7} _{-4.8}	0.17	4.63	28.67
SO687	0.8	0.73	-1.21	0.44	-7.94	412.8 ^{+4.2} _{-4.3}	0.06	5.52	25.22
SO694	0.1	0.16	-2.51	0.12	-8.82	392.3 ^{+9.2} _{-9.6}	0.13	4.85	40.2
SO697	0.2	0.97	-3.11	0.67	-10.05	404.5 ^{+2.4} _{-2.4}	0.51	3.66	30.15
SO726	0.6	0.56	-2.19	0.59	-9.15	403.9 ^{+6.8} _{-7.0}	0.1	5.03	–
SO736	0.1	1.49	-1.48	0.55	-8.23	401.0	1.03	3.05	29.9
SO739	0.1	0.1	-3.06	0.1	-9.35	433.3 ^{+20.3} _{-22.3}	1.02	3.06	–
SO774	0.0	0.49	-2.75	0.7	-9.84	403.3 ^{+3.3} _{-3.4}	1.28	2.86	31.17
SO818	0.4	0.29	-2.11	0.78	-9.36	405.4 ^{+4.1} _{-4.2}	2.37	2.32	18.11
SO823	1.5	0.32	-2.43	0.77	-9.66	401.0	1.37	2.79	36.7
SO844	0.7	0.62	-1.37	0.44	-8.14	415.5 ^{+3.7} _{-3.8}	2.18	2.39	29.22
SO848	0.0	0.02	-3.51	0.17	-10.47	356.3 ^{+16.3} _{-18.0}	0.46	3.75	–
SO859	0.6	0.41	-1.72	0.29	-8.31	407.9 ^{+6.4} _{-6.6}	0.84	3.22	25.15
SO897	0.6	0.85	-1.34	0.7	-8.33	401.0	0.77	3.29	23.56
SO927	0.6	0.33	-1.92	0.65	-9.03	413.6 ^{+4.7} _{-4.8}	1.0	3.07	20.72
SO984	0.1	0.72	-3.5	0.64	-10.46	409.6 ^{+3.1} _{-3.2}	1.18	2.92	27.4
SO1036	0.7	0.53	-0.89	0.59	-7.86	395.0 ^{+3.4} _{-3.5}	1.19	2.92	31.23
SO1075	0.6	0.14	-1.38	0.3	-8.22	390.0 ^{+8.2} _{-8.6}	1.6	2.66	–
SO1152	0.8	0.61	-1.26	0.58	-8.19	398.6 ^{+3.8} _{-3.9}	2.71	2.21	30.1
SO1153	1.5	0.33	0.02	0.9	-7.3	396.6 ^{+4.2} _{-4.3}	1.68	2.62	30.25
SO1154	1.8	0.08	-0.78	0.62	-8.19	401.0	1.64	2.64	31.6
SO1155	0.6	1.45	-0.92	0.86	-7.94	401.0	1.81	2.55	29.6
SO1156	0.4	0.66	-1.26	0.74	-8.33	403.8 ^{+2.6} _{-2.6}	2.42	2.3	28.15
SO1248	0.0	0.18	-3.3	0.13	-9.6	398.4 ^{+7.6} _{-7.9}	2.47	2.28	–
SO1260	0.0	0.15	-1.94	0.19	-8.53	386.3 ^{+6.2} _{-6.4}	1.95	2.49	35.6
SO1266	0.0	0.07	-4.76	0.15	-11.36	399.1 ^{+10.4} _{-11.0}	2.24	2.37	42.6
SO1267	0.6	0.76	-1.85	0.43	-8.57	400.5 ^{+5.2} _{-5.3}	2.42	2.3	27.65
SO1274	0.0	0.68	-0.98	0.64	-7.95	407.3 ^{+2.7} _{-2.7}	2.42	2.3	28.05
SO1327	0.1	0.33	-1.91	0.21	-8.32	397.7 ^{+5.7} _{-5.8}	2.79	2.18	33.15
SO1361	0.5	0.47	-0.61	0.46	-7.46	406.0 ^{+3.9} _{-4.0}	2.5	2.27	21.01
SO1362	0.0	0.1	-2.96	0.13	-9.37	399.4 ^{+10.2} _{-10.7}	2.76	2.19	35.85
SO1369	0.0	1.26	-1.45	0.57	-8.24	402.5 ^{+2.5} _{-2.5}	3.05	2.1	30.3